Journal of Energy Storage 52 (2022) 104747

Contents lists available at ScienceDirect

Journal of Energy Storage

journal homepage: www.elsevier.com/locate/est

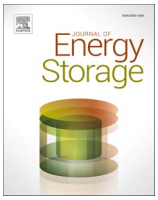

Research papers

Equivalent circuit definition and calendar aging analysis of commercial $Li(Ni_xMn_yCo_z)O_2$/graphite pouch cells

Hector Beltran [a,*], Pablo Ayuso [a], Nuria Vicente [b,c], Braulio Beltrán-Pitarch [a], Jorge García-Cañadas [a], Emilio Pérez [a]

[a] Department of Industrial Systems Engineering and Design, Universitat Jaume I, Av. Sos Baynat s/n, Castelló de la Plana 12071, Spain
[b] Department of Chemical Engineering, Universitat Jaume I, Av. Sos Baynat s/n, Castelló de la Plana 12071, Spain
[c] University Institute of Ceramic Technology (IUTC), Universitat Jaume I, Av. Sos Baynat s/n, Castelló de la Plana 12071, Spain

ARTICLE INFO

Keywords:
Lithium-ion battery
Aging mechanism
Accelerated aging tests
Impedance model

ABSTRACT

Aging-induced degradation of commercial Li-ion pouch cells with lithium nickel-manganese-cobalt-oxide-based cathodes and graphite anodes is studied at various operating conditions (temperature and voltage) by galvanostatic measurements and in situ electrochemical impedance spectroscopy (EIS). A detailed equivalent electrical circuit model, capable to fit the measured EIS spectra, is developed and validated. The work also confirms the capacity fade dependence of the calendar-aged cells on stress factors such as temperature and state-of-charge. The retained capacity is found to decrease linearly with $t^{0.5}$. However, it stands out that the degradation registered for cells held at 95% state-of-charge is lower than that for those at 70% and for the cases when temperatures are between 25 °C and 37.5 °C, which is a not very common singularity. A high performing calendar aging model is introduced accordingly. Both the electrical circuit model defined and the accurate calendar aging model developed provide useful tools for battery management systems in order to monitor and control both the state-of-health and the state-of-charge of these commercial cells.

1. Introduction

Li-ion batteries (LIBs) together with pumped-hydro (PH) installations are considered nowadays the leading energy storage (ES) technologies to be used to accumulate electricity and complement the massive penetration of intermittent renewable energy sources promoted by the Paris Agreement in order to achieve decarbonisation by 2050 [1]. Analysing both technologies, clear geographical and physical limitations are identified for PH beyond huge grid applications. This paves the way to LIBs as the flagship ES solution for applications where energy density is critical, ranging from portable consumer devices to electric vehicles [2].

Currently, there are six consolidated families of LIBs under commercialization worldwide, being the market clearly dominated by three of them: nickel-manganese-cobalt-oxide (NMC), nickel–cobalt–aluminum- oxide (NCA) and lithium iron-phosphate (LFP) batteries [3]. However, beyond the great effort being devoted to the development of new active materials (at both the cathode and the anode levels), better electrolyte formulations (introducing solid-state and polymeric proposals), and optimizations of the working conditions in the last 20 years [4], all the families of LIBs still present limitations in terms of energy density and lifetime [5,6]. Moreover, due to the non-linear nature of the chemical reactions taking place within the LIB cells during operation, the precise determination of certain key operational parameters, that have to be monitored continuously by the battery management systems (BMS) standing out the state-of-charge (SoC) [7,8] and the state-of-health (SoH) [9,10], remains a challenging task. This is even more important in a moment in which there is an open discussion about the best cell to implement in the skyrocketing industry of the electric vehicle. Until now, long-range EVs models have often prefered NCM or NCA cells but, due to safety and liability reasons, the much safer but less energy dense LFP alternative is on the rise [11].

Under this scenario, a great attention is being paid to develop techniques, methodologies, and mathematical models aiming at the proper estimation of both SoC and SoH at every type of cell. Electrochemical Impedance Spectroscopy (EIS) is probably the main technique used for non-destructive diagnosis tests [12] and lately used to characterize and model the aging phenomena of LIBs [13]. EIS measurements make it

* Corresponding author.
E-mail address: hbeltran@uji.es (H. Beltran).

https://doi.org/10.1016/j.est.2022.104747
Received 14 July 2021; Received in revised form 20 April 2022; Accepted 22 April 2022
Available online 6 May 2022

possible to discern between the different battery components and internal reactions, since each of them presents a characteristic frequency of response [14]. Different studies implementing this technique to characterize LIBs are available [15–17]. Some of them are indeed focused on NMC/graphite Li-ion cells [18], which being the most shipped chemistry, has concentrated an important part of the research. For instance, authors in [19] evaluated the degradation of 20 Ah NMC Li-ion pouch cells under light and heavy-duty real-life operating conditions. Or even [20] in which the cycle aging of commercial 40 Ah NMC/graphite pouch cells was studied at different cycling temperatures. Also, accelerated degradation tests combined with galvanostatic charge-discharge cycles devoted to analyse both calendar and cycle aging are introduced in the literature [21–24]. Calendar aging occurs when a battery is at rest condition, i.e. no current flows through the LIBs, whereas cycle aging takes place while the battery is being charged or discharged. In this sense, a very interesting work on calendar aging is introduced in [25]. It provides a comprehensive survey on the Li-ion calendar aging research from the past twenty years of commercially available LIB with different cathode and anode chemistries. Other works are focused on specific cells, like [26] in which the authors analyse the calendar aging of 16 Ah NMC/graphite pouch cells by means of Post-Mortem techniques, or the one in [27] where the authors tested 24 cylindrical 3,5 Ah NMC nickel-rich cells and analyzed the influence of the cells' self-discharge currents on the voltage imbalance of a battery pack, taking the calendar aging under consideration. A similar approach is introduced in [28] to study the impedance change and the capacity fade of other commercial 18650 NMC cylindrical cells. This work concludes that the additional charge throughput experienced by the cells due to the periodic electrochemical characterization induces significant cell degradation effects that impact the calendar aging study. Therefore, the calendar aging of this family of Li-ion cells has been extensively studied during the last years. However, to our knowledge, commercial 63 Ah high-energy capacity pouch cells have not been characterized in detail so far and their calendar aging has not been reported.

This work analyses the response of such commercial NMC/graphite pouch cells and defines a novel equivalent electrical circuit (EEC) that fits with high accuracy the spectra obtained by means of EIS measurements at different SoC values. The EEC structure selected had been previously used to study half-cells [29,30], whose behavior could not be defined by a diffusion element because some intermediate-frequency distortions usually arise in the form of an arc appearing just before the low-frequency capacitive behaviour. However, this work confirms this EEC as a valid model to describe and study the behavior of these full-cells. Also, the cells are subjected to different stress factors (temperature of 25 °C, 37.5 °C and 50 °C, and SoC of 20%, 40%, 75% and 95%) for more than a year. The periodic testing (including EIS and galvanostatic profiles) performed to each of the 24 cells under study allowed to analyse the evolution of the EEC parameters, and also to derive a mathematical calendar aging model. This provides a highly accurate aging diagnosis to be potentially used to estimate the calendar degradation of these commercial cells during their resting periods. This would allow a BMS to optimize the charging timing and even activate some refrigeration to prevent the battery pack from avoidable degradation.

This paper is organized as follows: Section 2 introduces the experimental setup together with the test matrix and the periodical measurement procedure performed to the cells. In Section 3, the resulting equivalent circuit and the calendar aging model are presented and discussed. Some concluding remarks are finally introduced in Section 4.

2. Experimental design

The test focuses on the commercial energy dense NMC pouch cells, model JH3, manufactured by LG Chem, Fig. 1. These cells present a non-disclosed stoichiometry cathode made of lithium-nickel-manganese -cobalt-oxide as active material and a graphite anode. They are manufactured by means of a lamination and vertical stacking process of the

Parameter	Value	Unit
Nominal capacity	63	Ah
Nominal energy	233	Wh
Nominal voltage	3.7	V
Voltage range	3.0 to 4.2	V
Energy density	412	Wh/l
Specific energy	198	Wh/kg
Storage temperature	-30 to 60	°C
Weight	1,175	g
Volume	565	mL
Dimension (W/L/T)	100.2 / 352.5 / 16.0	mm
Cathode active material	NMC	-
Anode material	Graphite	-

Fig. 1. JH3 NMC pouch cell proof by LG Chem. Technical specifications.

cathode, anode and separator, instead of the usual winding process, which according to LG Chem improves their dimensional stability and life-cycle. Their rated capacity is 63 Ah and they are usually implemented in battery packs used for stationary applications.

In order to degrade the cells, they were subjected to different controlled and constant values of SoC and temperature during 400 days. A CCK series compact climatic chamber from Dycometal and two lab ovens (Indelab, model IDL.AI80) were used to control the temperature. The climatic chamber did not control the humidity but its use was required due to the low ambient operating temperature (25 °C) defined for some of the cells. Moreover, 12 calibrated digital voltage sources (RS PRO, model RS-3005D) fixed and monitored the voltage of the cells.

All the electrochemical characterization and the capacity measurements were conducted in a 4-probe configuration with a PGSTAT30 potentiostat from Metrohm Autolab BV equipped with a 10 A booster and a FRA2 impedance module. The potentiostat was controlled by Nova 1.11 software. Impedance spectra were fitted using Zview software from Scribner Associates Inc.

2.1. Calendar aging matrix

The aging experiments were completed on a total of 24 JH3 cells. These cells were initially characterized as received (fresh condition) by impedance spectroscopy and capacity profiles, and then they were set up at 12 different operational combinations of temperature and SoC for 400 days. Cells were paired in couples under each of these 12 operational frameworks. For each of the combinations, summarized in Table 1, one cell from each couple was used as reference cell (the even numbered cell). Reference cells were only tested every six months, an the other cells from the pair (odd numbered in Table 1) were tested at regular intervals every 4 weeks. The aim at dividing the cells in two groups (reference and monthly-tested cells) was to analyse the potential

Table 1
Test matrix of calendar aging conditions.

T/SoC	3.57 V (≈ 20%)	3.67 V (≈ 45%)	3.85 V (≈ 70%)	4.11 V (≈ 95%)
25 °C	C1 / C2	C3 / C4	C5 / C6	C7 / C8
37.5 °C	C9 / C10	C11 / C12	C13 / C14	C15 / C16
50 °C	C17 / C18	C19 / C20	C21 / C22	C23 / C24

effect on the aging that could be introduced by the check-up characterization frequency during the whole experiment, as studied for NMC cells in cyclindrical format in [28] or in prysmatic format in [31]. In this way, one cell in every pair is only tested once every six months and its resulting degradation can be compared to that of its twin cell tested six times over the same period.

Table 1 summarizes the test matrix and the characteristics of the operational combinations tested. Note on the one hand how the 24 NMC cells are split in three groups of eight cells each and stored at three constant temperatures: 25 °C, 37.5 °C and 50 °C. These values are selected with the intention to cover the usual range of operational temperatures experienced by cells within battery packs in most real-life stationary applications. Only the 50 °C framework is somehow beyond recommendations but it has been introduced to favour an accelerated aging and, therefore, to provide results that would enrich the analysis. On the other hand, the 8 cells at each temperature were wired in pairs and voltage-controlled at each of the 4 SoC levels: $3.57V(\approx 20\%)$, $3.67V(\approx 45\%)$, $3.85V(\approx 70\%)$, and $4.11V(\approx 95\%)$.

Also in this case, the SoC levels were defined trying to encompass all the voltage operational range of the cells, with separation of 25% among setpoints. Note that these setpoints are shifted towards the full charge state because it is more usual to have the batteries operating closer to 100% SoC than fully discharged. The corresponding voltage values to be fixed by the voltage source were defined according to the V-SoC characteristic measured for this type of cell.

2.2. Characterization procedure

The fresh cells were initially charged from 3% SoC up to 98% SoC. Then, they were fully discharged again to 3%. Both charge and discharge intercalated various EIS measurements along each process. After that, cells charged for a second time up to 98% and finally discharged until the SoC level assigned to each during the experiment (according to Table 1). All the power exchanges during the charging and discharging galvanostatic processes were carried out under a 0.1 C-rate. These initial cycles were performed with the objective of forming a stable SEI that would facilitate a successful subsequent cycling performance [32], and were profited to measure the initial actual capacity of each cell. Moreover, for an extra fresh cell (C25), this initial cycle was combined with a series of EIS measurements in order to check their influence on the retained capacity (in Ah) and also to generate the EEC model here developed.

After this initial test, the cells were characterized periodically. As previously indicated, the characterization period was either four weeks or six months depending on the cell group. At every periodic test, each cell underwent a new discharge-charge-discharge galvanostatic cycle (at 0.1 C) and was submitted to three EIS measurements at the corresponding SoC values. The whole test procedure and the different EIS test points performed throughout the cycle are represented in Fig. 2. According to it, the periodical characterization started with an initial check-up analysis of the cell by a first EIS measurement at the designated resting SoC of each cell. Then, the cells were discharged down until their cut-off terminal voltage, achieved at 3.41 V. This discharge action, as well as the rest of charge or discharge operations along the cycle, were conducted by applying a constant current equal to ±6.3 A (C-rate = 0.1). This value was selected to ensure the quasi-equilibrium state of the cell after the process and to minimize the potential impact that higher C-rates could introduce in the aging. Hence, after discharging down to that

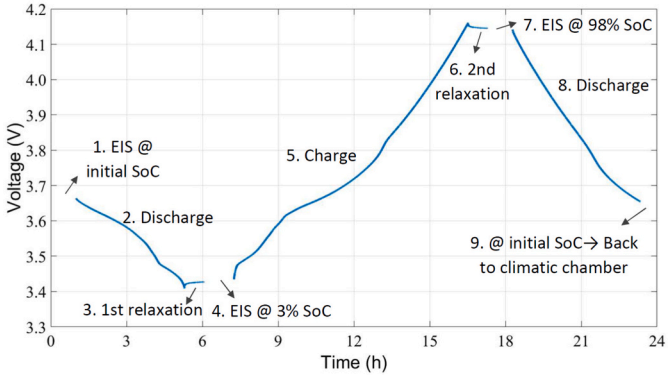

Fig. 2. Cell test procedure diagram.

cut-off voltage, a 45-minute relaxation period was introduced. This allowed the open circuit voltage (OCV) of the cells to recover to 3.425 V, which corresponds to a 3% SoC. At this point, a second EIS measurement was carried out. Then, an almost full charging process was conducted up to a terminal upper cut-off voltage of 4.16 V. Following the corresponding 45-minute relaxation period that allowed the OCV to softly drop down to 4.145 V (equivalent to a SoC equal to 98%), a third EIS measurement was performed. Finally, the cell was discharged again until it reached the initial SoC to be finally measured one more time and sent back to the climatic chamber or to the corresponding lab oven.

Regarding the EIS measurements, it is important to note that all of them were carried out galvanostatically, with a 5 A amplitude perturbation, in a frequency range from 500 Hz to 1 mHz. The cells underwent all these measurements and operations introduced periodically at room temperature (around 22 °C) and each test took around 23 h per cell.

3. Results and discussion

3.1. Equivalent circuit model determination

The EEC model definition was based on the results achieved for cell C25 in its initial characterization test. Fig. 3 shows the resulting voltage characteristic profiles as well as the corresponding incremental capacity/differential voltage (IC/DV) curves obtained for this cell. This characterization test started with an initial cell discharge down to 3% SoC. Then, the test proceeded with a galvanostatic charge cycle, up to the upper cut-off voltage of 4.16 V, and a discharge, down again to the low cut-off limit set at 3.41 V, as observed in Fig. 3a. The cell underwent various EIS measurements throughout both processes, marked as squares in Fig. 3a. Finally, a new charge process (red line) was performed and the capacity measured again to verify that the electrodes had not changed nor been damaged during the previous initial EIS measurements.

This initialization process was introduced to all the cells. The capacity registered during the second charging process varied from 57.68 Ah to 58.34 Ah, depending on the cell. No significant variations between the measurement during the EIS cycle and the measurement after them was registered for any cell. Thus, if the voltage range used for the test cycle is taken into account versus the whole operational range of these cells, calculations return a total extrapolated capacity for the 24 cells ranging from 60.7 Ah to 61.41 Ah, approaching their commercial rated values.

Regarding the specific results for cell C25, although it is quite difficult to infer the different reactions occurring within the cell at varying voltage levels from the voltage profiles represented in Fig. 3a, they can be split into three different sections: (i) below 3.50 V, with a significant voltage vs. capacity slope; (ii) between 3.50 and 3.70 V, where the slope of the curve flattens; and (iii) between 3.70 and 4.16 V, where the voltage linearly increases/decreases with the capacity. The shape of

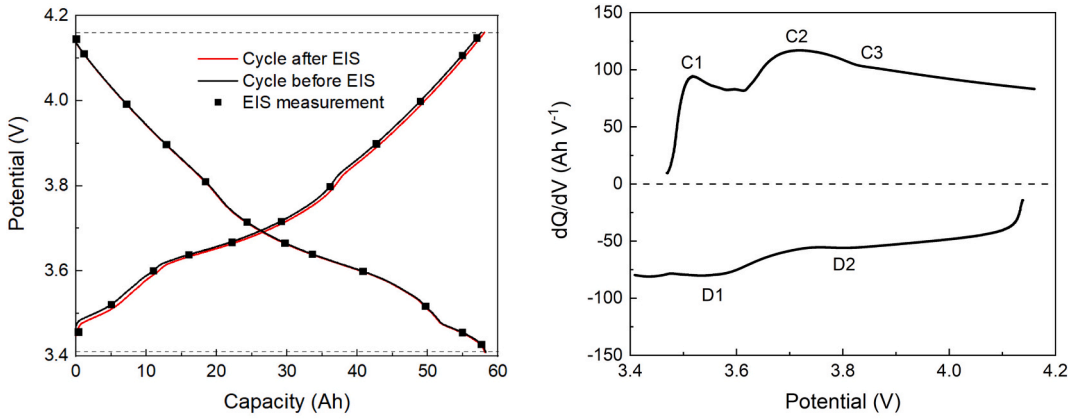

(a) (b)

Fig. 3. Results of the initial test performed to cell C25. (a) Selected potentials and charge state during the galvanostatic cycles; (b) IC/DV curves during the charge and the discharge process.

these curves is consistent with that previously reported for NMC cathodes vs. graphite anodes [33]. Besides, Fig. 3b displays the way the IC/DV evolves as a function of the operating cell voltage (V) for both the charging and the discharging process. It is important to remember that the area between the curve and the horizontal axis indicates the capacity that the cell admits at the corresponding voltage interval. Note how the voltage plateau in the charge/discharge curve in Fig. 3a now presents the typical NMC peaks in the IC/DV curve [34]. The peaks indicate different phase transitions at both anode and cathode (effects overlapped on the figure). Analyzing in detail the evolution of the IC/DV curves, a first sharp redox peak at 3.52 V (C1) followed by the main peak at 3.72 V (C2) during the charge reaction are mainly identified. These peaks correspond to the change in the oxidation state of Ni upon lithiation, which correlates with the flattened region of the voltage profiles in Fig. 3a. Authors in [35] associated C1 and C2 processes in NMC/graphite cells to the lithiation of graphite (C6 → LiC_x) and the H1 → M (rhombohedral to monoclinic) phase transition of the NMC cathode [36]. Then, around 3.80 V (C3), the M → H2 reversible phase transition takes place. Above it, the IC/DV rate decreases progressively until the voltage cut-off limit is reached. The IC/DV is always positive throughout this interval, which implies that some electrochemical reactions might be occurring. Although it is difficult to analyse them because the cut-off voltage of the test was too low, these reactions could be irreversible and potentially associated with the formation of both the SEI and the cathode electrolyte interface (CEI). Regarding the discharge reaction, only two clear peaks are observed. The predominant signal, observed at 3.54 V (D1), corresponds to the intermediate plateau in the galvanostatic discharge and is located at the same potential as C1. This comprehends both the phase transition M → H1 and the delithiation of graphite, which are the inverse reactions to those generating C1 and C2. On the other hand, D2 corresponds to the reversible H2 → M phase transition of the NMC at 3.80 V. Finally, note that due to the limited voltage range analyzed in this test, defined by the manufacturer in the safety datasheet to avoid irreversible damage to the cells during use, it was not possible to distinguish the peak below 3.40 V ascribed to the anode in the literature [33].

Some further insights can be introduced around the kinetic limitations inferred from the resistive processes occurring during the cell operation. They are derived from the Nyquist spectra plots obtained with the EIS measurements performed to the cell, and pointed out in Fig. 3a. The frequency response of the cells at four of the analyzed SoC is represented in Fig. 4a. Note how the Nyquist spectra exhibit two main features at different time constants associated with the corresponding specific electrochemical mechanisms: a semicircle obtained at high-frequencies (related to the electrode/electrolyte interfacial processes),

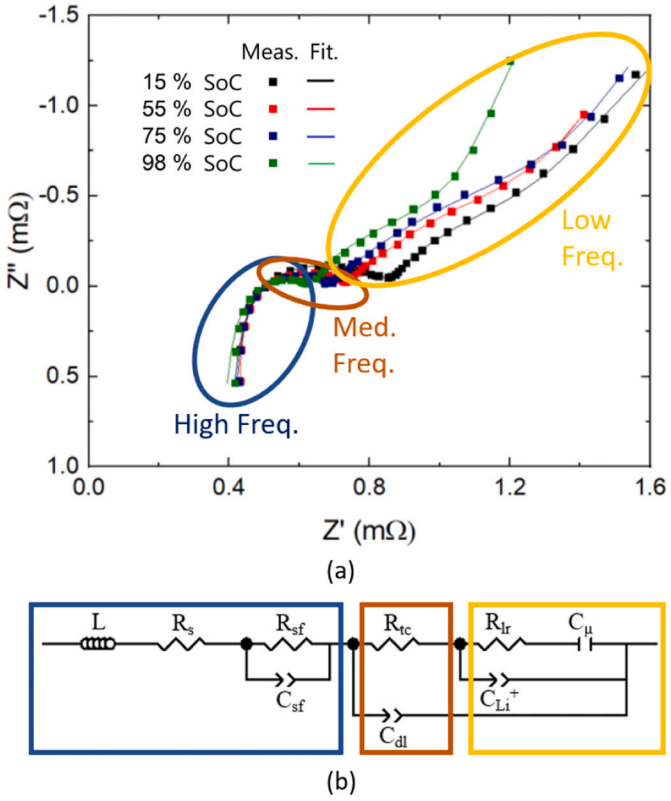

Fig. 4. (a) EIS Nyquist spectra at various SOCs; (b) developed EEC.

and a tilted line at low frequencies (that correlates to the mechanisms to store/deliver electrochemical energy). For the rest, the middle frequencies would correspond to the Li^+ diffusion process.

Taking into account these spectra, and after analyzing previous models described in the literature for NMC cathodes using Li metal as both the counter and the reference electrode [29,30], the proposal in this work is an EEC for these commercial NMC/graphite Li-ion cells as the one represented in Fig. 4b. This EEC fits the experimental impedance spectra with low error, as appreciated in the figure, and properly describes the physical and chemical processes (such as the electrochemical reactions, diffusion, migration of lithium and ohmic action) inside the cells.

Starting at high frequencies, the EEC includes an inductance, *L*,

which models the inductive behavior of the cell caused by its geometry and windings [37]. The parameter $L \approx 0.33\ \mu H$ is constant during both charge and discharge processes, and hardly influences the cell's performance [12,28]. Then, the EEC presents a resistance, R_s, which is ascribed to the ionic resistance of the electrolyte and to the electronic resistance of the current collectors [28,38]. This is known as the ohmic resistance and corresponds in Fig. 4a to the minimum value for the real part of the impedance, i.e. $R_s \approx 0.4\ m\Omega$. As frequency decreases, only one semicircle is observed in the Nyquist diagram while two would be expected [33]. This is due to the fact that the partial and individual effects at each electrode cannot be discerned separately. The first expected semicircle would be associated to the SEI layer and to the charge transfer at both electrodes. It has been previously reported that solid films are formed on lithiated transition-metal oxides (TMOs) because of the rich surface chemistry in alkyl carbonate electrolyte solutions and $LiPF_6$ salts [39]. In order to represent this part of the spectrum, a sub circuit formed by a resistance, R_{sf}, in parallel with a non-ideal capacitor (a constant phase element, CPE, with exponent defined between 0.8 and 1), C_{sf}, is used. The values registered for these parameters are $R_{sf} \approx 0.4\ m\Omega$ and $C_{sf} \approx 8\ F$, which also remain voltage independent.

At intermediate-to-high frequencies, the second overlapped semicircle would be related to the electrical processes at the active particles interface in both electrodes. This is defined by the charge-transfer resistance, R_{ct}, and by the double layer capacitance, C_{dl}, associated with the porosity of both graphite and NMC electrodes. This semicircle is rather voltage-independent, with $R_{ct} \approx 1.7\ m\Omega$ and the C_{dl} value mainly varying between 50 kF and 65 kF during both discharge and charge processes. In this case, C_{dl} represents again a non-ideal capacitor.

At low frequencies, the expected phenomena are a solid-state diffusion process and a capacitive behavior associated with the Li^+ storage into the anode. Therefore, due to the difficulty in associating this part of the resulting Nyquist spectra with a Warburg-like pattern (identified by slopes of 45 degrees in the diffusion tail), the proposed EEC just introduces a resistance, R_{lr}, in series with a capacitor, C_μ. R_{lr} is usually attributed to the different reaction rates limiting mechanisms inside the electrode particles, regardless of the underlying microscopic mechanism (ion diffusion and/or reaction), and C_μ represents the chemical capacitance. The transport limitations could be related to the solid-state diffusion of Li^+ ions within the host material or, also, to the hindrance of the resistive elements in electrochemical Li^+ alloying and conversion within the oxide matrices [15,38,40]. It should be equally noted that there is an additional capacitive behavior at low frequencies, modeled by the non-ideal capacitor C_{Li^+}, which is related to the Li^+ that have not reached the stable positions within the matrix yet [40,41]. This effect is observed in the change of the spectra near the elbow, distinguishing it from a Warburg classical pattern, followed by the true capacitive behavior, C_μ. The chemical capacitance is correlated with the differential change in the electrode charge upon voltage variation [41,42] and explains the ability of the oxide matrix to react with Li^+ ions.

Finally, in order to validate the consistency of the proposed EEC and its qualification to monitor the working conditions of the cells, two check-up actions were introduced. First, the resulting impedance values of the EEC with varying frequencies at each of the characterized SoCs were compared with the Nyquist spectra defined with the corresponding EIS measurements. Results for this comparison can be appreciated in the fitted lines in Fig. 4a and also on the 3D representation introduced in Fig. 5 for each the SoC levels taken into consideration during the initial test characterization. Note how the EEC model frequency response (solid line) perfectly reproduces all the experimental features measured (spheres), showing fitting errors for the parameters of the model below 10% all along the voltage range of the cell. Table 2 summarizes the values obtained for these parameters at various of the SoC (among all those measured and represented in Fig. 5) so that the model can be reproduced. The second check-up consist on comparing the chemical capacitance values obtained by the EIS with those calculated from the IC/DV curve. Results can be appreciated in Fig. 6. Note how the resulting C_μ presents a shape similar to that of the measured values as well as reaction peaks very close to those (C1 and C2) associated with the overall reversible reaction: $Li_x(Ni_y^{2+}Co_z^{3+}Mn_{1-y-z}^{4+})O_2 \leftrightarrow (Ni^{4+}Co^{4+}Mn^{4+})O_2 + xLi^+ + xe^-$ [42]. It should be noticed that a voltage shift between both curves arises, which is possibly due to the kinetic limitations that appear when the scan rates are not low enough during the continuous charging experiment, and this takes the system out-of-equilibrium. To sum up, the approach followed here enabled a proper differentiation between the two interfacial electrochemical processes and showed that it could be possible to monitor a commercial cell aging through EIS.

3.2. Aging evolution of the model parameters

The cells were periodically characterized according to the procedure introduced in Fig. 2. Therefore, new EIS measurements were routinely performed at three different SoC values: 3%, 98%, and the resting SoC of the cell. These measurements allowed us to analyse how the EEC model parameters evolved with time as a function of the storage temperatures

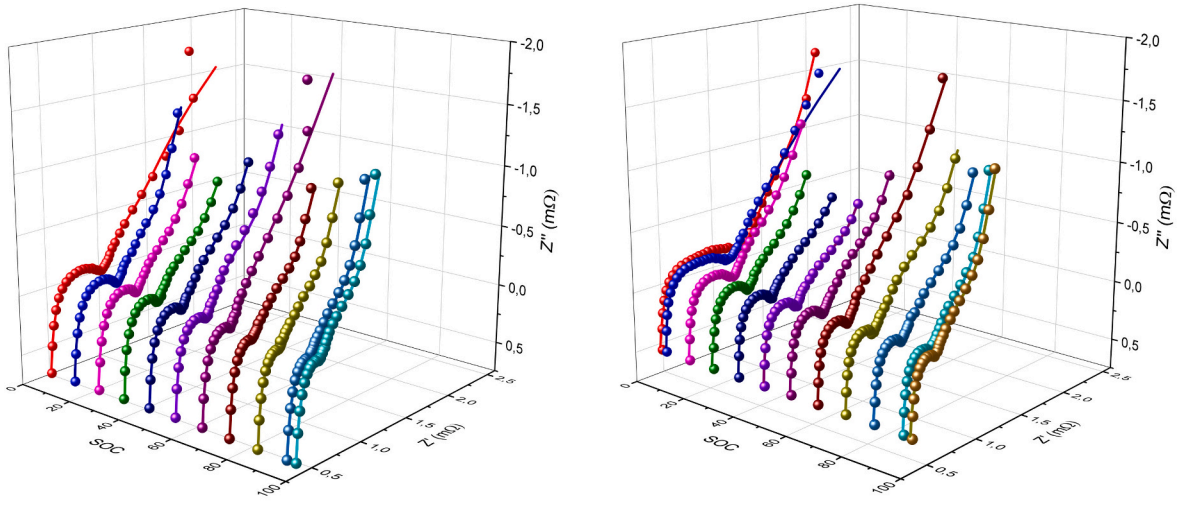

Fig. 5. 3D plot of the C25 cell Nyquist response spectra measured (spheres), and fitted model (lines), at the different SoC during the galvanostatic charge (a) and discharge (b).

Table 2
Obtained values for the parameters of the EEC model at various SoC.

	Charge					Discharge				
SOC	5%	25%	55%	75%	95%	95%	75%	55%	25%	5%
V(V)	3.46	3.60	3.72	3.90	4.11	4.11	3.90	3.72	3.60	3.46
L(μH)	0.34	0.34	0.33	0.33	0.34	0.34	0.33	0.33	0.33	0.34
R_s(mΩ)	0.3	0.4	0.4	0.4	0.4	0.4	0.4	0.4	0.4	0.4
R_{sf}(mΩ)	0.6	0.4	0.3	0.2	0.3	0.3	0.3	0.3	0.4	0.4
C_{sf}(F)	8.6	7.1	8.1	8.8	7.5	8.0	9.6	8.3	7.7	10.0
R_{ct}(mΩ)	1.1	2.0	1.9	1.5	1.3	1.4	2.1	1.2	1.0	1.2
C_{dl}(kF)	26.1	51.7	51.6	65.7	53.5	51.0	56.3	54.7	55.3	34
R_{Lr}(mΩ)	3.6	18.7	17.6	18.0	26.5	39.2	18.0	15.7	18.7	9.9
C_{Li+}(kF)	52.4	67.8	61.3	73.0	66.5	66.5	73.0	113	214	152
C_{μ}(kF)	125	222	187	219	177	177	218	276	275	171

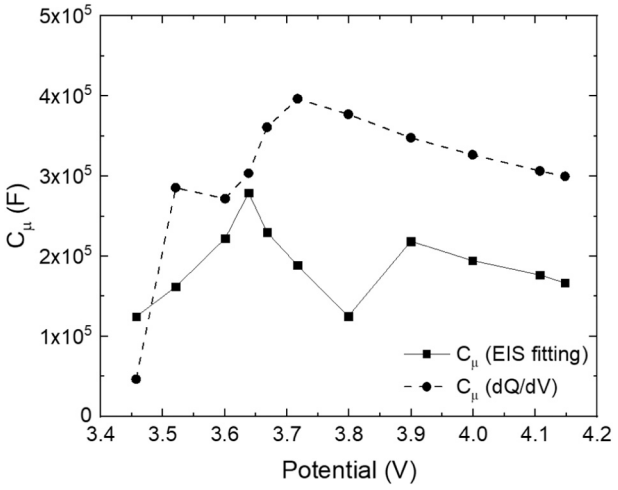

Fig. 6. Chemical capacitance of the JH3 cell obtained from -dQ/dV of the charge measurements at 0.1 C, and C_{μ} calculated for the EEC at the various EIS measurements.

and the resting SoC. The nine parameters from the model are divided into the 3 groups defined in the previous section as a function of the frequency ranges and represented in Fig. 4a: L, R_s, R_{sf}, and C_{sf} for high frequencies, R_{ct} and C_{dl} for medium frequencies, and C_{μ}, R_{lr} and C_{Li^+} for low frequencies.

Regarding the high frequency parameters, both L and C_{sf} showed a smooth increasing trend that ended up hardly doubling their values. On the contrary, although R_s was completely flat, R_{sf} even tended to decrease to around 50% of its initial value. Therefore, the overall resistive trend was towards reducing its value at these frequencies. However, although these changes constitute an evolution in relative terms, the absolute value of these parameters was kept so low that the cells' performances were not impacted. In fact, the most important change that would be expected according to previous works, an increase in R_s and R_{sf} as degradation advances and SEI grows [43], respectively, was not identified in this experiment. This can be associated to the high quality of the cells under analysis that did not significantly age during the calendar experiment. Harder operational conditions with hundreds of repeated cycling patterns should have been performed to be able to measure changes in R_s [44].

Concerning the medium frequency parameters, although the impedance should typically also increase with the aging in this frequency range [44], mainly due to the effect of the charging and discharging processes on the charge transfer capability and on the double layer, both R_{ct} and C_{dl} remained quite constant in our analysis too. In fact, since only 12 cycles were performed throughout the calendar aging experiment, the R_{ct} values persisted within the same order of magnitude during the whole study even for the cells subjected to the most extreme conditions (C23 and C24). When comparing their values with those obtained for the cells subjected to lower temperatures, it can be verified that lower values were identified, in the order of $0.1m\Omega$. Meanwhile, the C_{dl} values also persisted practically constant with a slight decrease when increasing storage temperature.

Finally, in relation to the parameters used to emulate the low frequencies response, it stands out that both R_{lr} and C_{Li^+} also present a flat evolution. No large changes are registered in their values for the different cells. Only the case of C_{μ}, representing the chemical capacitance, presents a noticeable reduction. This is barely null for cells C1 and C2 while the reduction achieves values of around 20% for cells C23 and C24, in agreement with the different capacity reductions experienced by each of the cells and introduced in the coming section.

It can be concluded that, in opposition to the results obtained by other authors such as Schmitt et al. in [28], which analyse in their work the calendar aging of 18650 NMC cylindrical cells, the degradation experienced by the JH3 pouch cells in our study is not significant. Nearly no increase of the ohmic and total polarization resistances is recorded with storage duration, and the whole cell impedance is basically unaltered along the experiments. Also, it is important to highlight that no significant differences were appreciated between the two groups of cells (periodically tested and reference cells). This implies that the impact of both the electrochemical characterization and the 10 extra galvanostatic cycles introduced at each check up to the periodically tested cells, with regard to those in the reference group, was negligible over the calendar aging.

3.3. Calendar aging model

The periodic tests performed also provided information on the retained capacity that the different cells presented along the experiment. Fig. 7 shows the capacity fade evolution experienced by each of the 24 cells stored at the three different temperatures (50 °C, 37.5 °C, and 25 °C, respectively) and four resting SoC levels. Results on each graph show the retained capacity values measured (during the charge performed from 3% to 98% SoC) for the four periodically tested cells (represented by continuous colored lines with dots) and for the four reference cells (represented by independent triangles) at the corresponding test temperatures. Also, colored dashed lines represent the linear dependence trend with $t^{0.5}$ in each of the graphs. Note how the linear relation is confirmed, based on the high R^2 values obtained in the fitting done for most of the cells. Only for cells at temperatures of 25°C and 37.5°C and SoC of 20% and 45% these R^2 values are low. This is due to the also low degree of aging experienced by these cells during the experiment. It is also important to highlight the importance of the anode overhang reversible effect, identified by other authors for NMC an LFP cells in previous works such as [45,46], respectively. This could be responsible for the capacity increase registered for low SoC cells after the initial capacity check up. Finally, note that the aging of the cells is clearly dependent on the SoC level in agreement with the literature (the greater the SoC the greater the aging). However, this general trend is broken by

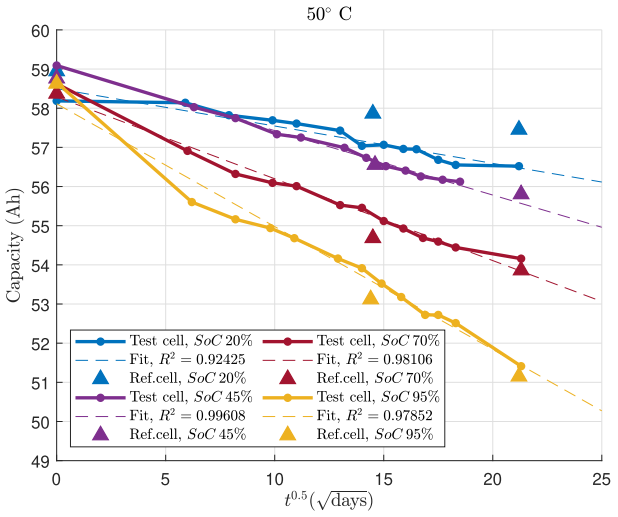

(a)

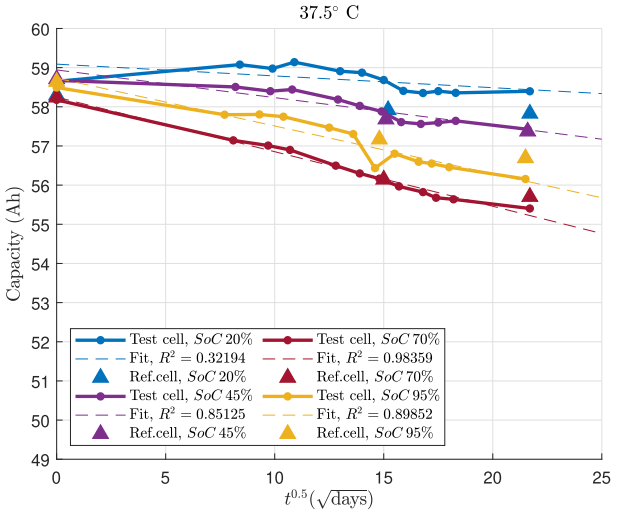

(b)

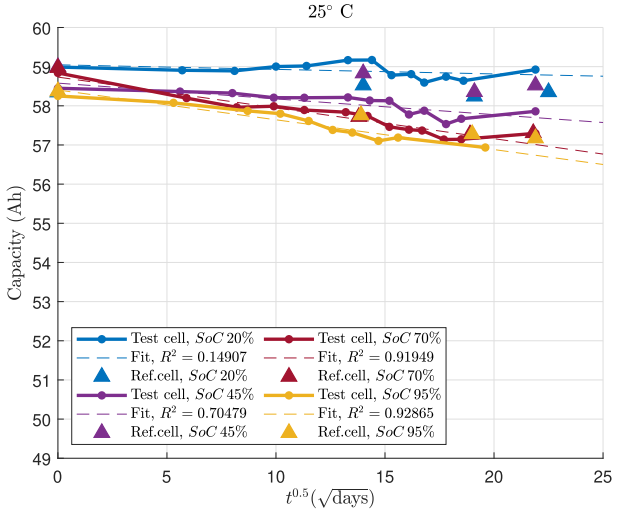

(c)

Fig. 7. Linear dependence of the measured retained capacity on $t^{0.5}$ at (a) 50 °C, (b) 37.5 °C, and (c) 25 °C.

the cells at 25 °C or 37.5 °C and SoC of 70% and 95%. Contrary to expectations, the aging expercienced by cells resting at 95% SoC is similar or even lower than that at 70% SoC. This surprising behavior was also obtained for the reference cells, C14 and C16, showing the sooner (at 70% SoC) lower retained capacity than the latter (at 95% SoC) at their third check-up test (12 months after the beginning of the experiment). The phenomenon was already somehow anticipated, although not discussed, by other authors in [25]. These two facts allows us to confirm the special and interesting response of this type of commercial cells at high SoC.

Similar results can be observed in Fig. 8 which respresents in this case the retained capacity measurements at each temperature and SoC versus time (in days), and connects them by the corresponding fitted surface. The evolution of the capacity fade with time during the experiment can be clearly observed.

Based on the retained capacity data of these cells, a semi-empirical lifetime model can be developed. Such models represent mathematical descriptions of the aging processes taking place within cells as a function of a combination of stress factors. In terms of calendar aging, the stress factors are the storage temperature and the resting SoC. According to some previous works, both stress factors influence the aging on the basis of the Eyring's law [47]. This law extends the Arrhenius law, often used to predict the time-to-fail as a function of temperature, to other stress factors such as voltage. In the Eyring law, each additional stress factor is added to the exponential function [48]. Similar recent proposals also identify an exponential or even a polynomial relation between those stress factors and the calendar aging [49]. We have analyzed the accuracy of up to 8 different mathematical models that combine polynomial and exponential relations, which are listed and specified in Table 3.

The first model, taken as reference, was already published for NMC cells in [50]. For the others, number 7 stands out due to its high R^2 value and its low root-mean-square error (RMSE). Therefore, this is the semi-empirical mathematical model proposed to estimate the calendar aging experienced by the commercial pouch cells under analysis.

The retained capacity estimation obtained with this model, for each of the combinations of stress factors analyzed, is also represented in Fig. 8. Note in this sense the colored continuous lines displayed together with the surfaces connecting the experimental measurements. Note how the model projections fit the experimental measurements quite accurately, with the exception of the aforementioned region at 25 °C or 37.5 °C and high SoC levels. At these temperatures, this figure shows again how they retain a similar or even more capacity when resting at 95% SoC than at 70% SoC, breaking the usual trend identified in the literature for most of the Li-ion cell types. This non-linearty is very difficult to model with semi-empirical mathematical models trying to cope with all the potential operation conditions of the cells. Therefore, taking into account this peculiarity, the model is accepted because its liability ascend to a $R^2 = 0.943$ value and a $RMSE = 0.635$, when that peculiar region is not considered. In conclusion, we determine the calendar aging process of NMC/graphite pouch cells is properly estimated by the proposed model.

4. Conclusions

This work analyzed the calendar aging experienced by JH3 commercial pouch NMC/graphite Li-ion cells from LG Chem. To do it, 24 cells were subjected to regular and periodic testing to evaluate their status while being aged at three different resting temperatures and four different states-of-charge. Tests consisted of EIS measurements at different SoC levels and a complete galvanostatic charge-discharge cycle.

EIS spectra obtained in the initial tests performed to fresh cells were fitted by an equivalent electrical circuit model which adapted the measured data and represented the internal effects of the cells, such as: the ohmic resistance, the polarization resistances, the capacitive effects and the diffusion processes. The evolution of parameters in the

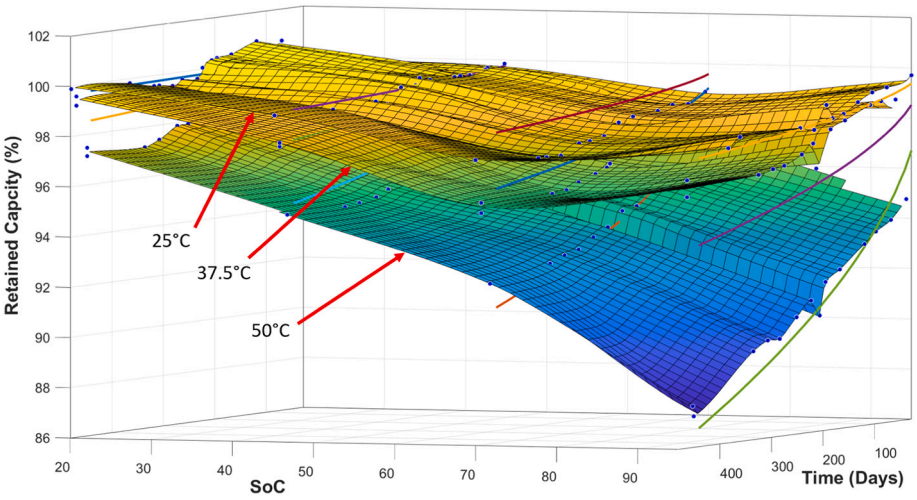

Fig. 8. Measured retained capacity at each temperature (surfaces) and resulting estimations of retained capacity (colored lines) obtained with aging model number 7.

Table 3
Mathematical models analyzed to characterize the calendar aging.

Model	Equation for $C_{fade}(V, T, t)$	α	β	γ	R^2	RMSE
0	$\alpha \cdot (V-\gamma) \cdot e^{-\beta/T} \cdot t^{0.75}$	3.02×10^6	6976	3.15	0.8273	1.079
1	$\alpha \cdot (V-\gamma) \cdot e^{-\beta/T} \cdot t^{0.75}$	3.02×10^6	6976	3.3	0.7342	1.353
2	$\alpha \cdot (V-\gamma) \cdot e^{-\beta/T} \cdot t^{0.75}$	3.02×10^6	6976	3.0	0.7671	1.255
3	$\alpha \cdot (V-\gamma) \cdot e^{-\beta/T} \cdot t^{0.75}$	1.082×10^6	6337	3.51	0.6845	1.480
4	$\alpha \cdot (V-\gamma) \cdot e^{-\beta/T} \cdot t^{0.5}$	4.237×10^6	6355	3.51	0.8282	1.085
5	$\alpha \cdot V^{\gamma} \cdot e^{-\beta/T} \cdot t^{0.5}$	0.013	6319	13.425	0.7610	1.281
6	$\alpha \cdot V^{\gamma} \cdot e^{-\beta/T} \cdot t^{0.75}$	0.0028	6300	13.543	0.6290	1.603
7	$\alpha \cdot SoC^{\gamma} \cdot e^{-\beta/T} \cdot t^{0.5}$	4004	6396	1.414	0.9091	0.781
8	$\alpha \cdot SoC^{\gamma} \cdot e^{-\beta/T} \cdot t^{0.75}$	978	6377	1.424	0.8233	1.102

equivalent circuit model was analyzed versus aging. The ohmic and the polarization resistances were found to remain constant during the experiment. In fact, no significant changes were registered in any of the parameters due to the relatively low number of cycles submitted to the cells, and only the chemical capacitance decreased, in agreement with the degree of degradation of each cell. In this regard, it is also important to sentence that the impact of the electrochemical characterization over the aging was negligible in our experiment. This is concluded from the null difference obtained in the results for the cells regularly tested every month and those for the reference cells tested every six months.

The galvanostatic cycles provided information on the capacity fade experienced by the cells throughout the experiment. These results allowed to define a semi-empirical calendar aging model including temperature and state-of-charge as stress factors. The capacity of the studied cells decreased linearly with $t^{0.5}$, being t the experiment time. As expected, the degradation was higher at higher storage temperatures and higher resting state-of-charge values. However, the latter was not observed at intermediate temperatures. Results at 25 °C and 37.5 °C showed how the degradation was similar, or even higher, at a state-of-charge of 70% than at a state-of-charge of 95%. This was an interesting result to be taken into account during the use and operation of this type of cells. Beyond that specificity, the calendar aging model proposed reproduced the measured results with high accuracy ($R^2 = 0.943$ and $RMSE = 0.635$), providing a useful tool to monitor and control both the state-of-health and the state-of-charge of these commercial cells.

Declaration of competing interest

The authors declare that they have no known competing financial interests or personal relationships that could have appeared to influence the work reported in this paper.

Acknowledgment

This work derives from the project “Anàlisi experimental i caracterització de l'envelliment de bateries de liti NMC” (reference GV-2019-087) funded by the Generalitat Valenciana. N. Vicente acknowledges Universitat Jaume I (UJI) through the Postdoctoral Fellowship Program (POSDOC/2020/04). The authors would like to also thank the cooperation provided by the Institute of Advanced Materials at UJI.

References

[1] United Nations, The Paris Agreement. Report of the Conference of the Parties to the United Nations Framework Convention on Climate Change (21st Session, 2015: Paris) vol. 4, 2015. https://unfccc.int/documents/184656.
[2] M. Armand, P. Axmann, D. Bresser, M. Copley, K. Edström, C. Ekberg, D. Guyomard, B. Lestriez, P. Novák, M. Petranikova, W. Porcher, S. Trabesinger, M. Wohlfahrt-Mehrens, H. Zhang, Lithium-ion batteries – current state of the art and anticipated developments, J. Power Sources 479 (Dec 2020), https://doi.org/10.1016/j.jpowsour.2020.228708.
[3] I. Tsiropoulos, D. Tarvydas, N. Lebedeva, Li-iosn batteries for mobility and stationary storage applications, in: JRC Science for Policy Report, EU Commission, 2018, https://doi.org/10.2760/87175.
[4] T. Placke, R. Kloepsch, S. Dühnen, M. Winter, Lithium ion, lithium metal, and alternative rechargeable battery technologies: the odyssey for high energy density, J. Solid State Electrochem. 21 (7) (Jul 2017), https://doi.org/10.1007/s10008-017-3610-7.
[5] J.B. Goodenough, Y. Kim, Challenges for rechargeable Li batteries, Chem. Mater. 22 (3) (Feb 2010), https://doi.org/10.1021/cm901452z.
[6] D. Deng, Li-ion batteries: basics, progress, and challenges, Energy Sci. Eng. 3 (5) (Sep 2015), https://doi.org/10.1002/ese3.95.
[7] Z. Li, J. Huang, B.Y. Liaw, J. Zhang, On state-of-charge determination for lithium-ion batteries, J. Power Sources 348 (Apr 2017), https://doi.org/10.1016/j.jpowsour.2017.03.001.
[8] S.-C. Huang, K.-H. Tseng, J.-W. Liang, C.-L. Chang, M. Pecht, An online SOC and SOH estimation model for lithium-ion batteries, Energies 10 (4) (Apr 2017), https://doi.org/10.3390/en10040512.

[9] M. Dubarry, G. Baure, D. Anseán, Perspective on state-of-health determination in lithium-Ion batteries, J. Electrochem. Energy Convers. Storage 17 (4) (Nov 2020), https://doi.org/10.1115/1.4045008.

[10] X. Tan, D. Zhan, P. Lyu, J. Rao, Y. Fan, Online state-of-health estimation of lithium-ion battery based on dynamic parameter identification at multi timescale and support vector regression, J. Power Sources 484 (Feb 2021), https://doi.org/10.1016/j.jpowsour.2020.229233.

[11] S. Ge, R.S. Longchamps, T. Liu, J. Liao, Y. Leng, C.-Y. Wang, High safety and cycling stability of ultrahigh energy lithium ion batteries, cell reports physicalScience 2 (10) (2021), https://doi.org/10.1016/j.xcrp.2021.100584.

[12] E. Barsoukov, J.R. Macdonald, Impedance Spectroscopy: Theory, Experiment, and Applications, John Wiley & Sons, 2018, https://doi.org/10.1002/0471716243.

[13] P. Iurilli, C. Brivio, V. Wood, On the use of electrochemical impedance spectroscopy to characterize and model the aging phenomena of lithium-ion batteries: a critical review, J. Power Sources 505 (2021), https://doi.org/10.1016/j.jpowsour.2021.229860.

[14] M. Gaberšček, Impedance spectroscopy of battery cells: theory versus experiment, Curr. Opin. Electrochem. (2021), https://doi.org/10.1016/j.coelec.2021.100917.

[15] N. Vicente, M. Haro, G. Garcia-Belmonte, New approaches to the lithiation kinetics in reaction-limited battery electrodes through electrochemical impedance spectroscopy, Chem. Commun. 54 (9) (2018), https://doi.org/10.1039/C7CC08373D.

[16] I.J. Gordon, S. Grugeon, H. Takenouti, B. Tribollet, M. Armand, C. Davoisne, A. Débart, S. Laruelle, Electrochemical impedance spectroscopy response study of a commercial graphite-based negative electrode for Li-ion batteries as function of the cell state of charge and ageing, Electrochim. Acta 223 (Jan 2017), https://doi.org/10.1016/j.electacta.2016.12.013.

[17] S. Skoog, S. David, Parameterization of linear equivalent circuit models over wide temperature and SOC spans for automotive lithium-ion cells using electrochemical impedance spectroscopy, J. Energy Storage 14 (Dec 2017), https://doi.org/10.1016/j.est.2017.08.004.

[18] Y. Olofsson, J. Groot, T. Katrasnik, G. Tavcar, Impedance spectroscopy characterisation of automotive NMC/graphite Li-ion cells aged with realistic PHEV load profile, in: 2014 IEEE International Electric Vehicle Conference (IEVC), IEEE, 2014, https://doi.org/10.1109/IEVC.2014.7056095.

[19] M.S. Hosen, D. Karimi, T. Kalogiannis, A. Pirooz, J. Jaguemont, M. Berecibar, J. Van Mierlo, Electro-aging model development of nickel-manganese-cobalt lithium-ion technology validated with light and heavy-duty real-life profiles, J. Energy Storage 28 (Apr 2020), https://doi.org/10.1016/j.est.2020.101265.

[20] K. Jalkanen, J. Karppinen, L. Skogström, T. Laurila, M. Nisula, K. Vuorilehto, Cycle aging of commercial NMC/graphite pouch cells at different temperatures, Applied Energy 154 (Sep 2015), https://doi.org/10.1016/j.apenergy.2015.04.110.

[21] P.Shafiei Sabet, A.J. Warnecke, F. Meier, H. Witzenhausen, E. Martinez-Laserna, D. U. Sauer, Non-invasive yet separate investigation of anode/cathode degradation of lithium-ion batteries (nickel–cobalt–manganese vs. graphite) due to accelerated aging, J. Power Sources 449 (Feb 2020), https://doi.org/10.1016/j.jpowsour.2019.227369.

[22] X. Cong, C. Zhang, J. Jiang, W. Zhang, Y. Jiang, A hybrid method for the prediction of the remaining useful life of lithium-ion batteries with accelerated capacity degradation, IEEE Trans. Veh. Technol. 69 (11) (Nov 2020), https://doi.org/10.1109/TVT.2020.3024019.

[23] W. Diao, S. Saxena, M. Pecht, Accelerated cycle life testing and capacity degradation modeling of LiCoO2-graphite cells, J. Power Sources 435 (Sep 2019), https://doi.org/10.1016/j.jpowsour.2019.226830.

[24] M. Ecker, N. Nieto, S. Käbitz, J. Schmalstieg, H. Blanke, A. Warnecke, D.U. Sauer, Calendar and cycle life study of li (nimnco) o2-based 18650 lithium-ion batteries, J. Power Sources 248 (2014) 839–851, https://doi.org/10.1016/j.jpowsour.2013.09.143.

[25] M. Dubarry, N. Qin, P. Brooker, Calendar aging of commercial Li-ion cells of different chemistries – a review, Curr. Opin. Electrochem. 9 (Jun 2018), https://doi.org/10.1016/j.coelec.2018.05.023.

[26] A. Iturrondobeitia, F. Aguesse, S. Genies, T. Waldmann, M. Kasper, N. Ghanbari, M. Wohlfahrt-Mehrens, E. Bekaert, Post-mortem analysis of calendar-aged 16 Ah NMC/graphite pouch cells for EV application, J. Phys. Chem. C 121 (40) (Oct 2017), https://doi.org/10.1021/acs.jpcc.7b05416. Retrived December.

[27] I. Zilberman, S. Ludwig, A. Jossen, Cell-to-cell variation of calendar aging and reversible self-discharge in 18650 nickel-rich, silicon–graphite lithium-ion cells, J. Energy Storage 26 (Dec 2019), https://doi.org/10.1016/j.est.2019.100900.

[28] J. Schmitt, A. Maheshwari, M. Heck, S. Lux, M. Vetter, Impedance change and capacity fade of lithium nickel manganese cobalt oxide-based batteries during calendar aging, Journal of Power Sources 353 (Jun 2017), https://doi.org/10.1016/j.jpowsour.2017.03.090.

[29] K.-J. Park, B.-B. Lim, M.-H. Choi, H.-G. Jung, Y.-K. Sun, M. Haro, N. Vicente, J. Bisquert, G. Garcia-Belmonte, A high-capacity positive electrode with a dual concentration gradient for next-generation lithium-ion batteries, J. Mater. Chem. A 3 (44) (2015), https://doi.org/10.1039/C5TA05657H.

[30] M. Haro, T. Song, A. Guerrero, L. Bertoluzzi, J. Bisquert, U. Paik, G. Garcia-Belmonte, Germanium coating boosts lithium uptake in Si nanotube battery anodes, Phys. Chem. Chem. Phys. 16 (33) (Jul 2014), https://doi.org/10.1039/C4CP02377C.

[31] M. Lewerenz, G. Fuchs, L. Becker, D.U. Sauer, Irreversible calendar aging and quantification of the reversible capacity loss caused by anode overhang, J. Energy Storage 18 (2018) 149–159, https://doi.org/10.1016/j.est.2018.04.029.

[32] E. Peled, S. Menkin, SEI: past, present and future, J. Electrochem. Soc. 164 (7) (2017) A1703, https://doi.org/10.1149/2.1441707jes.

[33] I. Landa-Medrano, A. Eguia-Barrio, S. Sananes-Israel, S. Lijó-Pando, I. Boyano, F. Alcaide, I. Urdampilleta, I. de Meatza, In situ analysis of NMC/graphite Li-ion batteries by means of complementary electrochemical methods, J. Electrochem. Soc. 167 (9) (2020) 90528, https://doi.org/10.1149/1945-7111/ab8b99.

[34] Y. Li, M. Abdel-Monem, R. Gopalakrishnan, M. Berecibar, E. Nanini-Maury, N. Omar, P. van den Bossche, J.Van Mierlo, A quick on-line state of health estimation method for Li-ion battery with incremental capacity curves processed by Gaussian filter, J. Power Sources 373 (Jan 2018), https://doi.org/10.1016/j.jpowsour.2017.10.092.

[35] R. Jung, M. Metzger, F. Maglia, C. Stinner, H.A. Gasteiger, Oxygen release and its effect on the cycling stability of (NMC) cathode materials for Li-ion batteries, J. Electrochem. Soc. 164 (7) (2017) A1361, https://doi.org/10.1149/2.0021707jes.

[36] L. de Biasi, B. Schwarz, T. Brezesinski, P. Hartmann, J. Janek, H. Ehrenberg, Chemical, structural, and electronic aspects of formation and degradation behavior on different length scales of Ni-rich NCM and Li-rich HE-NCM cathode materials in Li-ion batteries, Adv. Mater. 31 (26) (Jun 2019), https://doi.org/10.1002/adma.201900985.

[37] A. Maheshwari, M. Heck, M. Santarelli, Cycle aging studies of lithium nickel manganese cobalt oxide-based batteries using electrochemical impedance spectroscopy, Electrochim. Acta 273 (May 2018), https://doi.org/10.1016/j.electacta.2018.04.045.

[38] J. Song, M.Z. Bazant, Effects of nanoparticle geometry and size distribution on diffusion impedance of battery electrodes, J. Electrochem. Soc. 160 (1) (2012) A15, https://doi.org/10.1149/2.023301jes.

[39] R. Marom, S.F. Amalraj, N. Leifer, D. Jacob, D. Aurbach, A review of advanced and practical lithium battery materials, J. Mater. Chem. 21 (27) (2011) 9938–9954, https://doi.org/10.1039/C0JM04225K.

[40] F. Martinez-Julian, A. Guerrero, M. Haro, J. Bisquert, D. Bresser, E. Paillard, S. Passerini, G. Garcia-Belmonte, Probing lithiation kinetics of carbon-coated nanoparticle battery anodes, J. Phys. Chem. C 118 (12) (Mar 2014), https://doi.org/10.1021/jp412641v.

[41] J. Bisquert, Chemical capacitance of nanostructured semiconductors: its origin and significance for nanocomposite solar cells, Phys. Chem. Chem. Phys. 5 (24) (2003), https://doi.org/10.1039/b310907k.

[42] Y. Koyama, I. Tanaka, H. Adachi, Y. Makimura, T. Ohzuku, Crystal and electronic structures of superstructural, J. Power Sources 119-121 (Jun 2003), https://doi.org/10.1016/S0378-7753(03)00194-0.

[43] J.A. Gilbert, J. Bareño, T. Spila, S.E. Trask, D.J. Miller, B.J. Polzin, A.N. Jansen, D. P. Abraham, Cycling behavior of NCM523/graphite lithium-ion cells in the 3–4.4 V range: diagnostic studies of full cells and harvested electrodes, J. Electrochem. Soc. 164 (1) (Sep 2017), https://doi.org/10.1149/2.0081701jes.

[44] J. Zhu, M.S.Dewi Darma, M. Knapp, D.R. Sørensen, M. Heere, Q. Fang, X. Wang, H. Dai, L. Mereacre, A. Senyshyn, X. Wei, H. Ehrenberg, Investigation of lithium-ion battery degradation mechanisms by combining differential voltage analysis and alternating current impedance, J. Power Sources 448 (Feb 2020), https://doi.org/10.1016/j.jpowsour.2019.227575.

[45] M. Lewerenz, J. Münnix, J. Schmalstieg, S. Käbitz, M. Knips, D.U. Sauer, Systematic aging of commercial lifepo4— graphite cylindrical cells including a theory explaining rise of capacity during aging, J. Power Sources 345 (2017) 254–263, https://doi.org/10.1016/j.jpowsour.2017.01.133.

[46] B. Gyenes, D. Stevens, V. Chevrier, J. Dahn, Understanding anomalous behavior in coulombic efficiency measurements on li-ion batteries, J. Electrochem. Soc. 162 (3) (2014) A278, https://doi.org/10.1149/2.0191503jes.

[47] I. Baghdadi, O. Briat, J.-Y. Delétage, P. Gyan, J.-M. Vinassa, Lithium battery aging model based on Dakin's degradation approach, J. Power Sources 325 (Sep 2016), https://doi.org/10.1016/j.jpowsour.2016.06.036.

[48] E. Redondo-Iglesias, P. Venet, S. Pelissier, Eyring acceleration model for predicting calendar ageing of lithium-ion batteries, J. Energy Storage 13 (Oct 2017), https://doi.org/10.1016/j.est.2017.06.009.

[49] D. Galatro, C.D. Silva, D.A. Romero, O. Trescases, C.H. Amon, Challenges in data-based degradation models for lithium-ion batteries, Int. J. Energy Res. 44 (5) (Apr 2020), https://doi.org/10.1002/er.5196.

[50] D.-I. Stroe, M. Swierczynski, A.-I. Stan, R. Teodorescu, S.J. Andreasen, Accelerated lifetime testing methodology for lifetime estimation of lithium-ion batteries used in augmented wind power plants, IEEE Trans. Ind. Appl. 50 (6) (Nov 2014), https://doi.org/10.1109/TIA.2014.2321028.